GEOLOGY | THE GEOLOGICAL SOCIETY OF AMERICA®

https://doi.org/10.1130/G50503.1

Manuscript received 15 June 2022
Revised manuscript received 26 September 2022
Manuscript accepted 27 September 2022

Published online 2 December 2022

"Excess Ar" by laboratory alteration of biotite

Igor M. Villa[1,2] and Giulia Bosio[1]
[1]Dipartimento di Scienze dell'Ambiente e della Terra, Università di Milano Bicocca, 20126 Milan, Italy
[2]Institut für Geologie, Universität Bern, 3012 Bern, Switzerland

ABSTRACT

Many biotite phenocrysts from marine tephra layers have substoichiometric potassium concentrations and alkali occupation <<2.0 atoms per formula unit. Diagenetic alteration is an expected effect of exposure of fresh magmatic minerals to interstitial water and brine intrusions after the deposition and burial of sediments. To test the effect of diagenetic alteration on potassium-argon ages, we irradiated and step heated untreated Fish Canyon biotite (t = 28.2 Ma) and several aliquots leached to various extents in strong and weak acids. Laboratory alteration caused loss of K, age spectrum discordance, high step ages and total gas ages, Ar release at lower furnace temperature, higher Cl/K and Ca/K, and a slight decrease in ^{36}Ar concentration. Potassium loss was always higher than ^{40}Ar* loss. Electron microprobe element maps document that acids preferentially penetrated in phyllosilicate interlayers, removing K (and Na). Because Ar* is removed to a lesser extent than K, we propose that natural ^{40}K decay partly implants radiogenic Ar* into the tetrahedral-octahedral-tetrahedral (T-O-T) phyllosilicate layer, where Ar is shielded from interlayer leaching. The recoiled ^{39}Ar, which was produced by irradiation after the leaching, also partitioned between T-O-T and the interlayer; age spectrum discordance was probably enhanced by the heterogeneous partition of ^{39}Ar and ^{40}Ar* in leached samples.

INTRODUCTION

It has long been known that K-Ar analyses can give higher apparent ages than external constraints (Schaeffer and Zähringer, 1966). This "parentless" or "extraneous" ^{40}Ar has been found in mineral geochronometers in larger amounts than ^{40}Ar produced by the decay of ^{40}K in the independently known age of the mineral. A rigorous distinction between the two opposite origins of "extraneous" ^{40}Ar was proposed by Lanphere and Dalrymple (1976), who noted that "excess ^{40}Ar" ($^{40}Ar_{xs}$) was introduced, presumably by a fluid, into a mineral after its formation, but "inherited ^{40}Ar" ($^{40}Ar_{inh}$) was present in mineral precursors and was not completely lost during the formation of the presently observed minerals. As $^{40}Ar_{xs}$ relates to ^{40}Ar gain and $^{40}Ar_{inh}$ relates to ^{40}Ar loss (Villa et al., 2014, p. 817), the two kinds of extraneous Ar reflect two fundamentally different petrogenetic processes. The two terms were often confused in the later literature (e.g., Kelley, 2002), causing misunderstandings about the geologic processes recorded by the analyzed minerals. Estimation of a sample's true age despite extraneous ^{40}Ar has been attempted by numerous researchers; most efforts have been hampered by the difficulty in determining the extent of alteration, which is only indirectly inferred. With few exceptions (e.g., Wartho et al., 1996), very few studies have reported rigorous petrologic groundwork to discriminate between ^{40}Ar inheritance and externally derived $^{40}Ar_{xs}$. As combined microchemical and textural analyses are essential to pinpoint the mass balance of altered grain populations, most literature studies are only partially conclusive.

The impetus for our study was the suspected extraneous Ar in submarine tephras from the East Pisco Basin (Peru). Its Miocene sediments contain carbonate, diagenetic gypsum, anhydrite, and Mn minerals (Gariboldi et al., 2015; Gioncada et al., 2018; Bosio et al., 2019). Primary volcanic air-fall deposits are interbedded with biogenic siliceous and carbonate sediments. Volcanic feldspars from Pisco all have discordant ^{40}Ar/^{39}Ar age spectra and high Cl/K ($^{38}Ar_{Cl}/^{39}Ar_K$) ratios diagnostic of alteration, and they give apparent ages several million years older than coexisting biotite (Gariboldi et al., 2017). Biotite mostly gives flat age spectra ("plateaus") and low Ca/K ratios. However, in one instance of a horizontally continuous tephra, plateau ages of two stratigraphically equivalent samples differed by 0.071 ± 0.046 Ma, 2σ (Bosio et al., 2020). The biotite with a slightly lower K concentration gave both a higher K-Ar age and higher Cl/K, suggesting that ocean-floor alteration increased apparent ages.

Only one study (Kulp and Engels, 1963) reported laboratory experiments under controlled conditions. In Kulp and Engels' table 3, they quantified the effect of variably strong base exchange, where the K-Ar age of mica was lower than that of the starting material for very high K removal (>80%), but the treated mineral chronometers gave older ages for intermediate K removal (20%–50%).

In order to assess the role of alteration in increasing apparent ages, we performed two separate experiments on the same starting material, the Fish Canyon Tuff biotite (Hurford and Hammerschmidt, 1985), FCb, which was leached to very different intensities. The results described here credibly explain the observations from the Pisco tephras.

ANALYTICAL METHODS

In experiment A, two dry FCb aliquots were heated at 130 °C for 24 h in screw-top polytetrafluoroethane (PTFE) beakers: one in 6.4 *M* distilled HCl (A.1), one in 14.4 *M* distilled HNO_3 (A.2). They were abundantly rinsed in distilled water, dried, wrapped in Al foil, and irradiated at the McMaster University Research Reactor (MURR; McMaster University, Hamilton, Canada) together with an untreated aliquot (A.0) of the same starting material, carefully avoiding Cd shielding so as to preserve the information on $^{38}Ar_{Cl}$. The aliquots were analyzed by stepwise heating following the methods of Bosio et al. (2020). In experiment B, three dry FCb aliquots were subjected to more gentle leaching in screw-top PTFE beakers: two were heated at 130 °C for 24 h, one in distilled water (B.1) and one in 0.01 *M* HCl (B.2); one was leached at room temperature for 10 min in 6.4 *M* HCl (B.3). They were irradiated without Cd shielding at the MURR together with untreated aliquot

CITATION: Villa, I.M., and Bosio, G., 2023, "Excess Ar" by laboratory alteration of biotite: Geology, v. 51, p. 121–125, https://doi.org/10.1130/G50503.1

TABLE 1. BIOTITE COMPOSITIONS CALCULATED FROM $^{40}Ar/^{39}Ar$ SYSTEMATICS

Sample	Mass (mg)	Treatment	Molarity	[K] (%)	Rel. dep.	[Cl] (μg/g)	Rel. dep.	[Ca] (μg/g)	Rel. dep.	[40Ar*] (pL/g)	Rel. dep.	TGA (Ma)
A.0	8.0	None	–	7.9	–	1409	–	2516	–	8.81	–	28.2
A.1	5.2	Hot HCl	6.4	3.5	0.56	829	0.41	1364	0.58	4.54	0.49	33.6
A.2	5.2	Hot HNO_3	14.4	2.9	0.64	751	0.47	951	0.46	4.29	0.51	38.3
B.0	8.5	None	–	7.8	–	1952	–	1889	–	8.63	–	28.5
B.1	5.3	Hot H_2O	–	7.4	0.06	1984	–0.02	1777	0.06	8.66	–0.01	30.1
B.2	6.5	Hot HCl	0.01	7.0	0.10	1740	0.11	574	0.70	8.47	0.02	30.9
B.3	9.6	Cold HCl	6.4	6.7	0.14	1649	0.15	576	0.70	7.77	0.10	29.6

Note: The mass fractions of K, Cl, and Ca were calculated from the total ^{39}Ar, ^{38}Ar, and ^{37}Ar, respectively; "hot" and "molarity" refer to the employed acids (see Analytical Methods); "rel dep" is the depletion factor relative to the starting material. TGA—total gas age.

B.0. The complete $^{40}Ar/^{39}Ar$ data are shown in Table S1 in the Supplemental Material[1] and summarized in Table 1.

A few unirradiated grains of aliquot B.2, treated with dilute HCl, were analyzed by electron probe microanalysis (EPMA), following Bosio et al. (2020). The mica grains were mounted perpendicular to the (001) plane, exposing the inner part of the biotite platelets (Heri et al., 2014). Element maps were acquired for 15 individual grains with an electron beam diameter of 3 μm and a step size of 0.3 μm. Quantitative compositions were determined for 46 points chosen near the centers of the grains, avoiding the most obviously reacted rims, in order to assess if the apparent absence of reaction actually did reveal ingress of HCl. The EPMA results are shown in Table S2.

[1]Supplemental Material. Table S1 (complete Ar isotope data), Table S2 (electron microprobe data), and Figure S1. Please visit https://doi.org/10.1130/GEOL.S.21520959 to access the supplemental material, and contact editing@geosociety.org with any questions.

RESULTS AND DISCUSSION

In general, the choice of the obtained data that must be discussed in a publication depends on the authors' preconceived decision about the part of the data set that best constrains their interpretation. Because our laboratory treatment altered the mineral chronometer, the petrologic groundwork is as essential as the mass spectrometry results.

In both experiments, all artificially altered aliquots showed higher apparent ages than the untreated ones (Figs. 1A and 1B; Table S1). In experiment A, the age mismatch and the degree of internal discordance of the age spectra were higher than those in experiment B. Calculating the mass fractions of K, Cl, Ca, and $^{40}Ar^*$ (Table 1) revealed that the high apparent K-Ar ages were due to preferential leaching of K relative to Ar and to Cl, whereas Ca leaching was less uniform, possibly due to minute residues of the Ca-rich sediment matrix. Since Cl^- substitutes for OH^- in the tetrahedral-octahedral-tetrahedral (T-O-T) structure, it is intuitive that K is more readily removed than Cl when the interlayer is unzipped by leaching. A surprising result is that the relative Cl and $^{40}Ar^*$ depletions are similar to each other. This can be explained by proposing that both Cl and $^{40}Ar^*$ are located in the T-O-T, the former as bound anion substituting for OH^-, and the latter unbound but occluded, as its large atomic radius hinders it from passing through the tight cation-oxygen bonds.

Isotope correlation diagrams emphasize that the heating steps for which the chemical signature is furthest removed from that of the pristine aliquot are usually also those with the highest apparent age (Figs. 1C and 1D). The extent of the compositional variations correlates with the intensity of the acid leach. The oxidizing 14.4 *M* HNO_3 leach created greater compositional damage to the starting material than the 6.4 *M* HCl leach for the same leach duration.

Differential Ar release rates depend on the cohesiveness of the mineral structure. The Ar degassing rate can be quantified by the parameter k_R (Villa, 2021). The differential release plots show the temperature interval over which

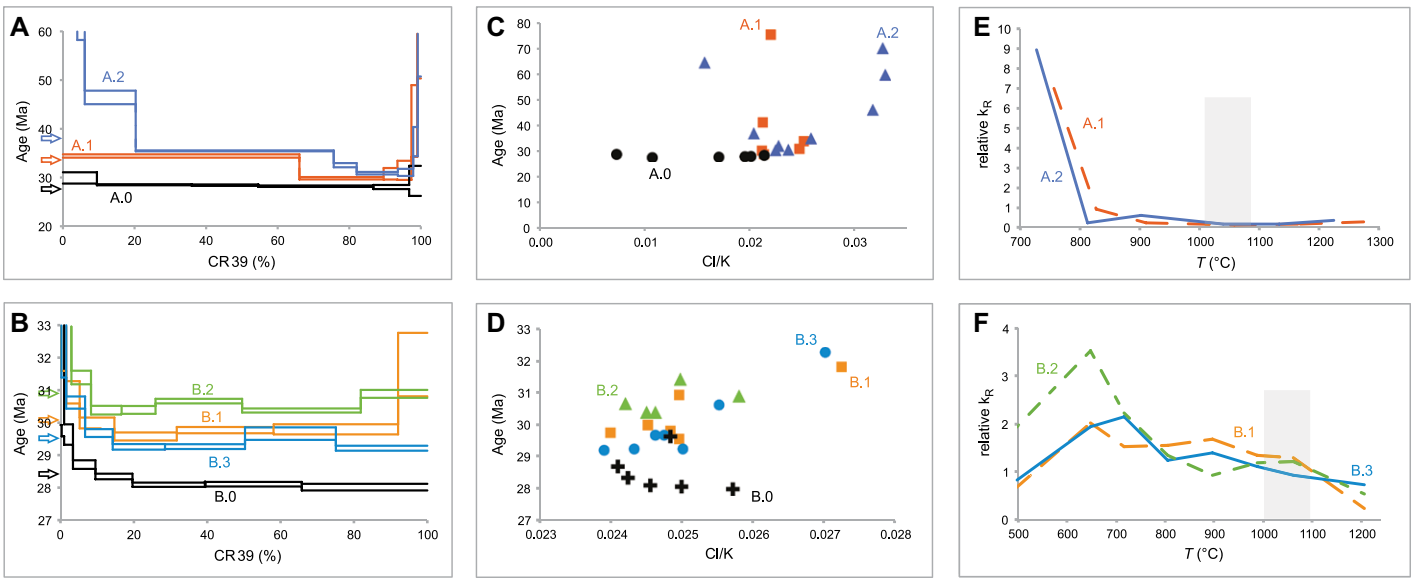

Figure 1. $^{40}Ar/^{39}Ar$ results. (A,B) Age spectra for experiments A and B, respectively. CR39 is cumulative ^{39}Ar release (%). Labels of aliquots are the same as in Table 1. Arrows to the left of the ordinate axis mark total gas ages from Table 1. (C,D) Common-denominator three-isotope correlation plots for experiments A and B, respectively. Note the change of scale. Points with the largest "excess age" anomalies are those with the highest Cl/K ratios. (E,F) Differential release plots for experiments A and B, respectively. Differential ^{39}Ar degassing rate, k_R, is normalized to that of an untreated aliquot. Values > 1 mean that leached biotite at that temperature degassed ^{39}Ar faster than the untreated aliquot. Gray band marks the peak of differential release in sample A.0.

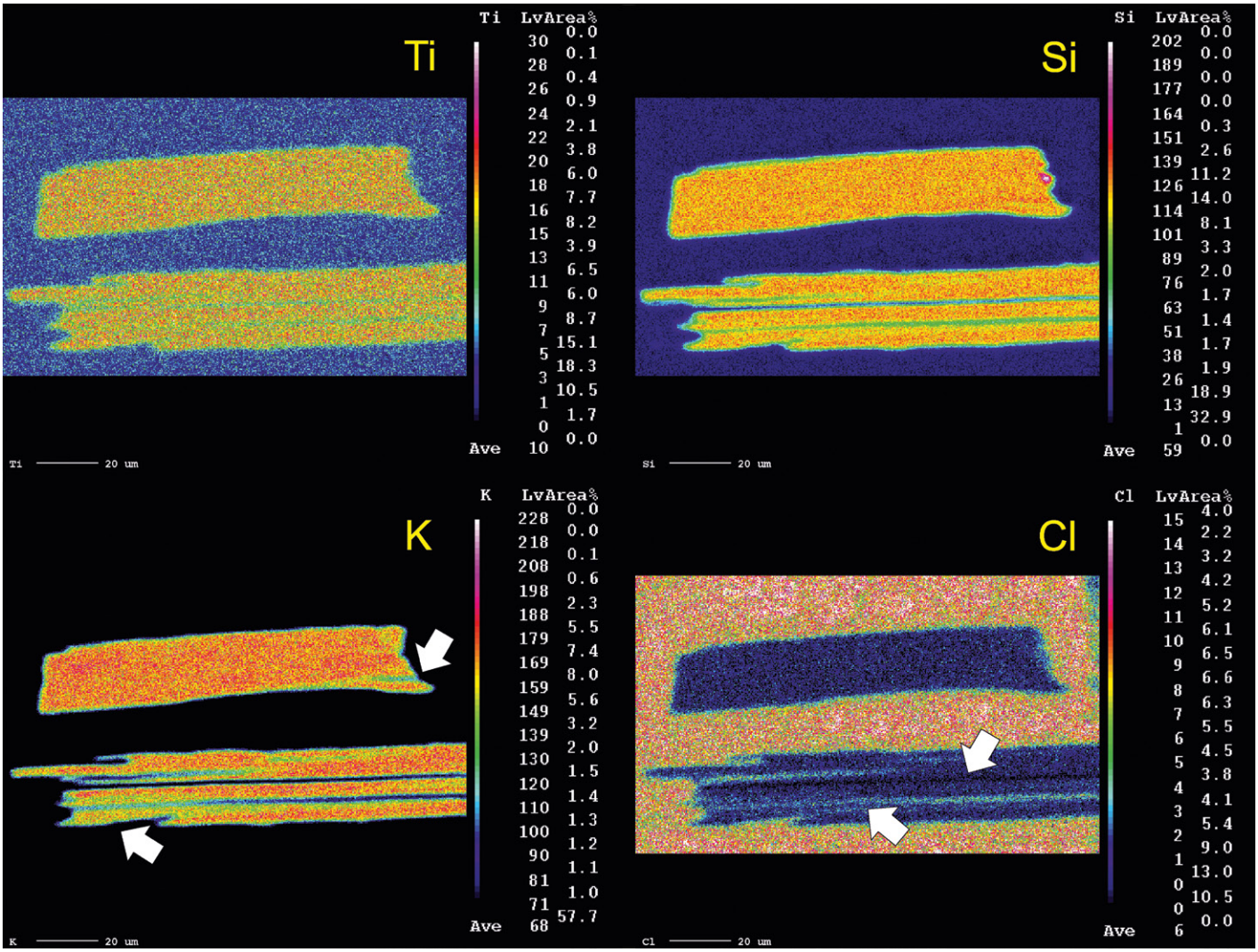

Figure 2. Element maps of biotite grain B.2.7, leached in hot dilute HCl, mounted perpendicular to (001). Scale bars = 20 μm. Each pixel corresponds to a chosen step size of 0.3 μm; the diameter of the electron beam was ~10 pixels. Arrows in the K map mark two patches showing localized K depletion. Arrows in the Cl map mark two contrasting compositions in cleavages: the upper one is devoid of all elements and probably originated from polishing after leaching; the lower one is enriched in Cl and depleted in K and Si, and it represents a reaction zone of mica with HCl and probable formation of talc (K-free T-O-T [tetrahedral-octahedral-tetrahedral]) and serpentine (T-O).

phyllosilicates dehydrate and concomitantly most efficiently release ^{39}Ar. In experiment B, in which structural degradation due to leaching was intentionally kept low, visual appreciation of small k_R variations is ineffective. We therefore normalized the differential release rate of each treated aliquot to that of the untreated reference. Figures 1E and 1F plot the temperature dependence of the relative differential release rate, k_R(A.1)/k_R(A.0), etc. The relative rate was much higher than 1 in experiment A (Fig. 1E) at low furnace temperature and dropped to <1 in high-temperature steps. This requires the structural collapse of samples A.1 and A.2 to have occurred at a lower temperature and to a more extreme degree than in reference sample A.0. This was also observed, to a lesser degree, in experiment B (Fig. 1F). The hot distilled water did modify the Ar release rate of aliquot B.1, but it had the smallest effect. The 24 h leach with hot dilute acid (B.2) modified k_R more than B.3, even if the K loss was lower (Table 1).

At first sight, EPMA element maps (Fig. 2; Fig. S1) for aliquot B.2 show unproblematic biotite. However, compositional data from total ^{39}Ar concentrations give an ~10% K loss from the bulk biotite (Table 1). Therefore, the maps ought to be screened in detail to find the minute depletions. The Ti map, an immobile element, shows very subdued relative variations (Fig. 2). The Si map shows two prominent bands parallel to the (001) plane, corresponding to cleavage planes, with a depletion $D \approx 30\%$ for the lower band and $D > 80\%$ for the upper band (Fig. 2). The reduced Si intensity could have two causes: (1) a true cleavage gap, where all major-element concentrations are zero, and the width is 5 pixels, i.e., 1.5 μm; or (2) a depleted reaction zone with incomplete removal of cations. Explanation 1 would point to mechanical damage during polishing, explanation 2 would be compatible with acid reaction that had occurred before polishing. The K distribution map shows two depletion bands coincident with the Si depletion, and additionally an ~20% depletion over an ~30-μm-sized patch (arrow at the bottom left), well distinct from the cleavage planes (Fig. 2). The arrow at the upper right, in the smaller biotite grain, shows a K depletion parallel to the (001) plane that is absent from the Si map. These images pinpoint the observed 10% bulk K depletion to micrometer-sized reaction patches. The Cl map (Fig. 2) supports both explanations for the Si and K depletion. The upper band of the Si map, marked by an arrow, has a vanishingly small Cl signal, as predicted by explanation 1. In contrast, the lower band (also marked by an arrow) has a three- to fivefold increase of the Cl signal, meaning that hot HCl found a pathway along a cleavage plane and leached away the

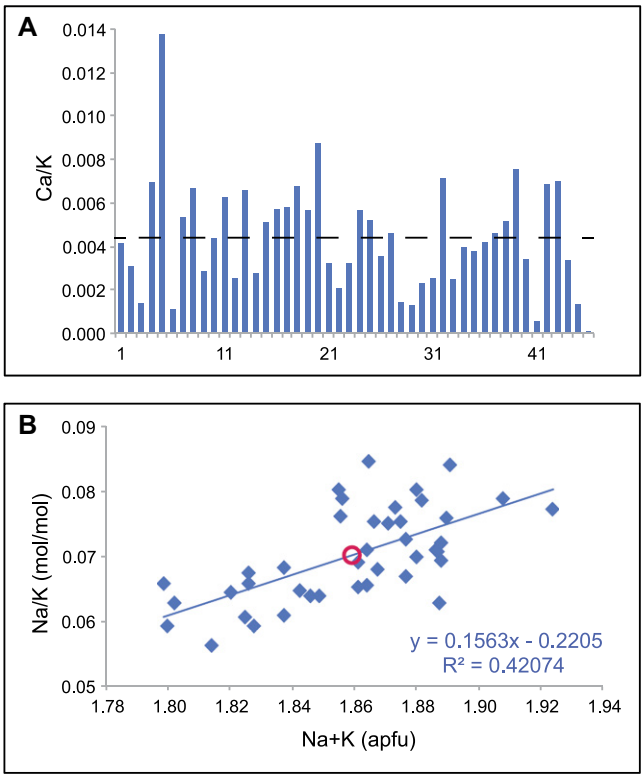

Figure 3. Electron probe microanalysis (EPMA) compositional data for 15 grains of sample B.2. (A) Ca/K ratio. Variation range of the EPMA analysis (between 0.001 and 0.014) is much more subdued than the variation range of stepwise heating analysis (between 0 and 0.07 ± 0.01). EPMA averages the signatures of minerals intergrown at a scale smaller than the beam diameter, whereas step heating can resolve them individually. (B) Comparison of Na and K loss in grain centers upon leaching. Most grain centers show detectable alkali loss, as HCl penetrated patchily into entire grain. Large open circle marks the average of *X* and *Y* values of analyzed spots. Positive correlation is evidence that most pristine biotite patches have high alkali occupation and a high Na/K ratio; progressive removal of alkalis from interlayer site preferentially depletes Na.

soluble elements, K and partly also Si, forming first talc layers and then serpentine layers, both heavily enriched in Cl, over a width of ~2 μm. Similar patterns are visible in Figures S1A–S1C. The K depletion and Cl enrichment observed by EPMA validate the conclusion derived from Figures 1C and 1D, which show that the high Cl/K ratios are a diagnostic hallmark of alteration.

A possible cause of excessively high $^{40}Ar/^{39}Ar$ ratios could in principle be recoil loss of ^{39}Ar (Smith and Huneke, 1976; Villa, 1997) during irradiation. Increased $^{40}Ar/^{39}Ar$ ratios were also discussed by Di Vincenzo et al. (2003), Smith et al. (2008), and Hall (2014).

Two arguments suggest that recoil is not the only cause of high apparent ages. (1) Stepwise leaching demonstrates (Villa et al., 2006) that hot, concentrated acids remove all alkali and earth alkali cations from micas; therefore, in experiment A, most of the missing ^{39}Ar is due to K removal rather than due to recoil. (2) In experiment B, the EPMA element maps show K and Na removal, often associated with Cl gain (Fig. 2). This does not rule out an additional contribution of recoil loss of ^{39}Ar to the observed K loss. However, the work by Smith and Huneke (1976) on an artificial mixture exclusively exhibiting ^{39}Ar recoil, without artificial K removal, predicted and observed that the low-temperature steps should give lowered ages due to re-implantation of recoiling ^{39}Ar. All aliquots of experiment B contradicted this behavior, as all low-temperature heating steps had excessively old apparent ages. This indicates that, even for experiment B, the main effect of artificial alteration was the net removal of alkali cations.

Two features of the quantitative EPMA spot analyses (Table S2) are shown in Figure 3. Figure 3A shows the Ca/K ratio measured by EPMA. Ca/K is not *per se* an indicator of alteration; it provides a comparison with that calculated from the $^{37}Ar/^{39}Ar$ ratio. This comparison points out the vastly different resolving power of the in situ analysis, which is limited by the size of the electron beam, 3 μm, and by the stepwise heating analysis, which reveals more extreme Ca/K variations between 0 and 0.07 ± 0.01 by exploiting the differential release properties of clay phases intergrown at a scale <3 μm. Figure 3B compares the behavior of alkali elements Na and K during acid leaching. The correlation line has a negative intercept and a slope >0; both of these features mean that the Na loss is even higher in all spots that record some K loss. If one assumes, purely for argument's sake, that the pristine mica has an alkali site occupation $x = 1.92$ atoms per formula unit and a Na/K molar ratio $y = 0.080$, then the most altered point, with $x = 1.80$ and $y = 0.061$, has lost 6.25% of its total alkalis and 24% of its Na. Within analytical uncertainty on the low Na mass fraction, points define a low-dispersion linear correlation, implying simple binary mixing between magmatic biotite and the alkali-depleted clay pseudomorph.

The fact that the centers of the grains did show detectable alkali loss means that the reaction front did not follow a regular concentric zoning. Acid was observed to exploit the interlayers to patchily penetrate into the entire grain (Fig. 2; Fig. S2).

Reconstruction of the age of the unaltered material only from the altered sample is challenging. Because micas give "plateaus" regardless of the intracrystalline age distribution (Foland, 1983; Hodges et al., 1994; Villa, 2021), unless the analyzed separate consists of different polytypes or compositions (Villa and Hanchar, 2017), the step ages of the treated aliquots cannot be easily back-extrapolated to the known age of the untreated aliquot. The most extensively altered patches are represented by the largest deviations from the bulk chemical signature in Figures 1C and 1D. In principle, the trend formed by the most and least altered patches could be used to infer the age of the pristine mica; however, in practice, the 28.2 Ma FCb age is never unambiguously constrained in this particular case.

CONCLUSIONS

(1) Bulk removal of K from the phyllosilicate interlayer by laboratory leaching is lower than that of Na but higher than that of $^{40}Ar^*$ and Cl.

(2) Altered mica is readily identified by its high $^{38}Ar_{Cl}/^{39}Ar_K$ ratio.

(3) The reduced removal of $^{40}Ar^*$ can only be explained if a part of the $^{40}Ar^*$ does not reside in the interlayer but has recoiled into the T-O-T mica structure and been shielded from acid leaching.

(4) The differential effect of even mild acid leaching on K and $^{40}Ar^*$ is one explanation of why biotite from marine tephra layers affected by high H_2CO_3 and Cl^- concentrations can show excessively high K-Ar ages.

ACKNOWLEDGMENTS

Valentina Barberini is warmly thanked for maintaining the mass spectrometer laboratory. The skill of Stephan Brechbühl was decisive in obtaining the grain mount. Andrea Risplendente is thanked for help with the microprobe analysis. Constructive criticism by three anonymous reviewers and editor Marc Norman helped us to improve our presentation.

REFERENCES CITED

Bosio, G., Gioncada, A., Malinverno, E., Di Celma, C., Villa, I.M., Cataldi, G., Gariboldi, K., Collareta, A., Urbina, M., and Bianucci, G., 2019, Chemical and petrographic fingerprinting of volcanic ashes as a tool for high-resolution stratigraphy of the Upper Miocene Pisco Formation (Peru): Journal of the Geological Society, v. 176, p. 13–28, https://doi.org/10.1144/jgs2018-071.

Bosio, G., Malinverno, E., Villa, I.M., Di Celma, C., Gariboldi, K., Gioncada, A., Barberini, V., Urbina, M., and Bianucci, G., 2020, Tephrochronology and chronostratigraphy of the Miocene Chilcatay and Pisco formations (East Pisco Basin, Peru): Newsletters on Stratigraphy, v. 53, p. 213–247, https://doi.org/10.1127/nos/2019/0525.

Di Vincenzo, G., Viti, C., and Rocchi, S., 2003, The effect of chlorite interlayering on ^{40}Ar-^{39}Ar biotite dating: An ^{40}Ar-^{39}Ar laser-probe and TEM investigations of variably chloritised biotites: Contributions to Mineralogy and Petrology, v. 145, p. 643–658, https://doi.org/10.1007/s00410-003-0472-z.

Foland, K.A., 1983, ^{40}Ar/^{39}Ar incremental heating plateaus for biotites with excess argon: Chemical Geology, v. 41, p. 3–21, https://doi.org/10.1016/S0009-2541(83)80002-3.

Gariboldi, K., Gioncada, A., Bosio, G., Malinverno, E., Di Celma, C., Tinelli, C., Cantalamessa, G., Landini, W., Urbina, M., and Bianucci, G., 2015, The dolomite nodules enclosing fossil marine vertebrates in the East Pisco Basin, Peru: Field and petrographic insights into the Lagerstätte formation: Palaeogeography, Palaeoclimatology, Palaeoecology, v. 438, p. 81–95, https://doi.org/10.1016/j.palaeo.2015.07.047.

Gariboldi, K., Bosio, G., Malinverno, E., Gioncada, A., Di Celma, C., Villa, I.M., Urbina, M., and Bianucci, G., 2017, Biostratigraphy, geochronology and sedimentation rates of the Upper Miocene Pisco Formation at two important marine vertebrate fossil-bearing sites of southern Peru: Newsletters on Stratigraphy, v. 50, p. 417–444, https://doi.org/10.1127/nos/2017/0345.

Gioncada, A., Petrini, R., Bosio, G., Gariboldi, K., Collareta, A., Malinverno, E., Bonaccorsi, E., Di Celma, C., Pasero, M., Urbina, M., and Bianucci, G., 2018, Insights into the diagenetic environment of fossil marine vertebrates of the Pisco Formation (late Miocene, Peru) from mineralogical and Sr-isotope data: Journal of South American Earth Sciences, v. 81, p. 141–152, https://doi.org/10.1016/j.jsames.2017.11.014.

Hall, C.M., 2014, Direct measurement of recoil effects on ^{40}Ar/^{39}Ar standards, *in* Jourdan F., et al., eds., ^{40}Ar/^{39}Ar Dating: From Geochronology to Thermochronology, from Archaeology to Planetary Sciences: Geological Society, London, Special Publication 378, p. 53–62, https://doi.org/10.1144/SP378.7.

Heri, A.R., Robyr, M., and Villa, I.M., 2014, Petrology and geochronology of the "muscovite standard" B4M, *in* Jourdan F., et al., eds., ^{40}Ar/^{39}Ar Dating: From Geochronology to Thermochronology, from Archaeology to Planetary Sciences: Geological Society, London, Special Publication 378, p. 69–78, https://doi.org/10.1144/SP378.2.

Hodges, K.V., Hames, W.E., and Bowring, S.A., 1994, ^{40}Ar/^{39}Ar age gradients in micas from a high-temperature–low-pressure metamorphic terrain: Evidence for very slow cooling and implications for the interpretation of age spectra: Geology, v. 22, p. 55–58, https://doi.org/10.1130/0091-7613(1994)022<0055:AAAGIM>2.3.CO;2.

Hurford, A.J., and Hammerschmidt, K., 1985, ^{40}Ar/^{39}Ar and K/Ar dating of the Bishop and Fish Canyon tuffs: Calibration ages for fission-track dating standards: Chemical Geology, v. 58, p. 23–32, https://doi.org/10.1016/0168-9622(85)90024-7.

Kelley, S.P., 2002, Excess argon in K-Ar and Ar-Ar geochronology: Chemical Geology, v. 188, p. 1–22, https://doi.org/10.1016/S0009-2541(02)00064-5.

Kulp, J.L., and Engels, J., 1963, Discordances in K-Ar and Rb-Sr isotopic ages, *in* Radioactive Dating: Vienna, Austria, International Atomic Energy Agency, p. 219–238.

Lanphere, M.A., and Dalrymple, G.B., 1976, Identification of excess ^{40}Ar by the ^{40}Ar/^{39}Ar age spectrum technique: Earth and Planetary Science Letters, v. 32, p. 141–148, https://doi.org/10.1016/0012-821X(76)90052-2.

Schaeffer, O.A., and Zähringer, J., 1966, Potassium Argon Dating: Heidelberg, Germany, Springer, 234 p., https://doi.org/10.1007/978-3-642-87895-4.

Smith, M.E., Singer, B.S., Carroll, A.R., and Fournelle, J.H., 2008, Precise dating of biotite in distal volcanic ash: Isolating subtle alteration using ^{40}Ar/^{39}Ar laser incremental heating and electron microprobe techniques: The American Mineralogist, v. 93, p. 784–795, https://doi.org/10.2138/am.2008.2517.

Smith, S.P., and Huneke, J.C., 1976, The realities of recoil: ^{39}Ar recoil out of small grains and anomalous patterns in ^{40}Ar-^{39}Ar dating, *in* Proceedings of the 7th Lunar Science Conference: Houston, Texas, Lunar and Planetary Institute, p. 1987–2008.

Villa, I.M., 1997, Direct determination of ^{39}Ar recoil range: Geochimica et Cosmochimica Acta, v. 61, p. 689–691, https://doi.org/10.1016/S0016-7037(97)00002-1.

Villa, I.M., 2021, The in vacuo release of Ar from minerals: 1. Hydrous minerals: Chemical Geology, v. 564, https://doi.org/10.1016/j.chemgeo.2021.120076.

Villa, I.M., and Hanchar, J.M., 2017, Age discordance and mineralogy: The American Mineralogist, v. 102, p. 2422–2439, https://doi.org/10.2138/am-2017-6084.

Villa, I.M., Ruggieri, G., Puxeddu, M., and Bertini, G., 2006, Geochronology and isotope transport systematics in a subsurface granite from the Larderello-Travale geothermal system (Italy): Journal of Volcanology and Geothermal Research, v. 152, p. 20–50, https://doi.org/10.1016/j.jvolgeores.2005.09.011.

Villa, I.M., Bucher, S., Bousquet, R., Kleinhanns, I.C., and Schmid, S.M., 2014, Dating polygenetic metamorphic assemblages along a transect through the western Alps: Journal of Petrology, v. 55, p. 803–830, https://doi.org/10.1093/petrology/egu007.

Wartho, J.A., Rex, D.C., and Guise, P.G., 1996, Excess argon in amphiboles linked to greenschist facies alteration in the Kamila amphibolite belt, Kohistan island arc system, northern Pakistan: Insights from ^{40}Ar/^{39}Ar step-heating and acid leaching experiments: Geological Magazine, v. 133, p. 595–609, https://doi.org/10.1017/S0016756800007871.

Printed in USA